Analysis of the influence of the wind speed profile on wind power production

Energy Reports 8 (2022) 8079–8092

Contents lists available at ScienceDirect

Energy Reports

journal homepage: www.elsevier.com/locate/egyr

Research paper

Analysis of the influence of the wind speed profile on wind power production

C.A. Lopez-Villalobos [a,*], O. Martínez-Alvarado [b], O. Rodriguez-Hernandez [c], R. Romero-Centeno [a]

[a] Instituto de Ciencias de la Atmósfera y Cambio Climático, Universidad Nacional Autónoma de México, Ciudad Universitaria, 04510, Mexico City, Mexico
[b] National Centre for Atmospheric Science, University of Reading, Department of Meteorology, Whiteknights Road, Earley Gate, Reading, RG6 6ES, United Kingdom
[c] Instituto de Energías Renovables, Universidad Nacional Autónoma de México, Priv. Xochicalco s/n, Col. Centro, Temixco, Morelos, CP 62580, Mexico

ARTICLE INFO

Article history:
Received 1 December 2021
Received in revised form 19 May 2022
Accepted 15 June 2022
Available online 28 June 2022

Keywords:
Vertical wind profile
Logarithmic profile
Similarity theory
Wind resource assessment
Surface boundary layer
Power law method
Atmospheric stability

ABSTRACT

The characterization of wind speed and its variability at a site is important for wind resource assessment. The most readily available wind measurements are at 10 m above ground level. These measurements can then be extrapolated vertically to estimate wind power production. In this work, the Monin–Obukhov similarity method was implemented to estimate the wind speed vertical profile within the surface boundary layer for a southeast Mexican site, considering seasonal and diurnal variations of the surface boundary layer stability parameters. Additionally, a power-law method was implemented where the wind shear exponent was set following the International Electrotechnical Commission (IEC) standard and using a variable wind shear exponent. The results showed that the log-law and the variable wind shear method produce better estimates than the IEC standard. The mean power production was estimated at hub height (80 m above surface level) using anemometric data from the Mexican Wind Atlas and then compared with that calculated using the equivalent wind speed estimated from variable wind shear exponent and log-law model. No influence of the vertical wind speed variation within and on top (up to 117.5 m) of the surface boundary layer was found on the mean power production for a wind turbine with a diameter of 90 m and a hub height of 80 m.

1. Introduction

The economic viability of wind power projects depends on the site's wind conditions since the wind farm's energy production has to compensate for the installation and maintenance cost. A reliable assessment of the wind resource is crucial to manage existing wind farms and evaluate the viability of future ones (Serban et al., 2020; Gormo et al., 2021). Therefore, modelling the vertical structure of the surface layer flow is required, especially the vertical wind speed profile, e.g., to extrapolate wind speed measurements performed at lower altitudes to the wind turbine's hub height. The wind shear magnitude is site-specific and depends on wind direction, wind speed, atmospheric stability, surface roughness, complexity of the terrain, and other atmospheric phenomena. Complex land areas are characterized for high shear and turbulence levels in the wind flow, although this could increase the wind turbine power and load fluctuations (Schulz et al., 2014). Complex terrains are usually avoided because of the more severe wind conditions but are becoming more appealing for the wind industry (Alfredsson and Segalini, 2017).

Vertical variation of wind speed is an important parameter for wind turbine design, especially for those with large diameter rotors. Several theoretical and empirical models have been developed to describe wind speed vertical distribution across the atmospheric boundary layer (Gualtieri, 2019a). Here, we use a logarithmic model and a power-law method. The wind speed profile is commonly described by a logarithmic profile valid close to the surface (diabatic surface layer wind profiles), modified by the Monin–Obukhov similarity theory (MOST) for thermal stability. In an ideal horizontally homogeneous terrain where the atmosphere is in a steady state, the surface layer turbulence properties are sufficiently approximated by the MOST (Obukhov, 1971; Monin and Obukhov, 1959). The similarity theory assumes that normalized variances and covariances of various atmospheric surface layer parameters are universal functions of a stability parameter governed by the Obukhov length. MOST agrees with measured data at least up to 100 m (Holtslag, 1984). According to the MOST, the profiles of wind and air temperature in the turbulent surface layer could be described by a set of equations

* Corresponding author.
E-mail address: calovi@atmosfera.unam.mx (C.A. Lopez-Villalobos).

https://doi.org/10.1016/j.egyr.2022.06.046

Nomenclature and abbreviations

IEC	International Electrotechnical Commission standard
AEM (by its acronym in Spanish)	Mexican Wind Atlas
log-law	Logarithmic law
MOST	Monin–Obukhov similarity theory
u_*	Friction velocity (m s^{-1})
z_0	Surface roughness length (m)
L	Obukhov length (m)
T	Air temperature (K)
P_0	Atmospheric reference pressure (Pa)
P	Air pressure (Pa)
r	Mixing ratio for unsaturated air (g/g)
k	Von Karman constant
z	Vertical height (m)
d	Zero plane displacement
Ri_m	Richardson number
T_0	Absolute air temperature at height z_1 (K)
z_m	Geometric mean height (m)
u_r	Reference wind speed (m s^{-1})
z_r	Reference and height (m)
P_T	Wind turbine power production (W)
V_{eq}	Rotor equivalent wind speed (m s^{-1})
A	Rotor disk swept area (m^2)
u_i	Wind speed measured in the given section (m s^{-1})
A_i	Area of a discretized section of the rotor disk (m^2)

Greek letters

α	Wind shear exponent
θ	Potential air temperature (K)
θ_v	virtual potential air temperature (K)
ψ_m	Stability correction function
ζ_m	Dimensionless heigh z/L
ϕ_m	Monin–Obukhov stability correction function

that depends only on a few parameters, including the surface roughness length z_0 (Kalnay, 2003). The surface roughness and the different atmospheric stability conditions greatly influence the vertical profile of winds. They must be taken into account in the estimation of the vertical wind profile (Radünz et al., 2020; Zhan et al., 2020; Chanprasert et al., 2020; Du et al., 2021). Wind speed and air temperature measurements at different heights can be used to derive the Monin–Obukhov length L via the Richardson number (Holtslag et al., 2014; Donnou et al., 2019; Holtslag et al., 2017). The Monin–Obukhov length L has to be derived from measurements at the site. The power-law method is one of the most used tools for extrapolating wind speed in the vertical direction. The power law is empirical and commonly used in wind engineering to define vertical wind profiles because it is simple and ready to use (Lopez-Villalobos et al., 2018; IEC61400-1, 2005; IEC61400-2, 2013). It describes the degree of atmospheric stability by means of the wind shear exponent, which indicates the amount of stratified flow, but it is not a direct measure of stability.

Surface layer turbulence properties over complex terrain are not satisfactorily understood despite several relevant studies (Martins et al., 2009; Rotach and Zardi, 2007; Moraes et al., 2005; Rotach et al., 2004; Nadeau et al., 2013; Tampieri, 2017; Serafin et al., 2018). Thus, there is still no consensus regarding the functional forms of MOST relationships or the limitations of this theory (Lee and Buban, 2020). Applications over flat sites are more frequent than elsewhere and implementation over complex terrains sites is generally more challenging because they can significantly affect the shear profile (Gualtieri, 2019b). As the air flows over complex terrains, changes occur to the mean and turbulent components of the flow which may result in a decrease or increase in wind shear, or even occurrences of negative wind shear (Wharton et al., 2015). Flow in the roughness sublayer (e.g. flow over vegetative canopies) resembled a turbulent mixing layer (Raupach et al., 1996), formed around the inflectional mean velocity profile, which develops between two coflowing streams of different velocities, differs in several ways from turbulence in a surface layer.

In addition to the aforementioned, wind speed profiling is useful for the development of wind resource atlases (Ouammi et al., 2010; Elliott et al., 1987; Archer and Jacobson, 2003), estimation of shear impacts on wind turbine loading and failures (Smith et al., 2002; Lopez-Villalobos et al., 2018), and wind farm layout optimization (Vasel-Be-Hagh and Archer, 2017; Roque et al., 2020; Gualtieri, 2017).

Given that wind speed profiles depend on atmospheric stability, this should not be assumed as constant throughout the day and year because this profile is used to assess the wind power production and wind turbine rotor loads (Lopez-Villalobos et al., 2018; Han et al., 2018). Some studies have been carried out to assess the impact of the atmospheric stability on resource assessment and wind turbine aerodynamic performance, and fatigue loads, e.g. Holtslag et al. (2014), Sathe and Bierbooms (2007), Rehman et al. (2018) and Sathe et al. (2013) showed the significance of atmospheric stability on wind turbine power production as well as on wind turbine loads, where it is directly caused by the influence of the underlying atmospheric stability on both wind shear and turbulence properties. Moreover, there are studies that indicate that blade loads were hardly affected by atmospheric stability (Kretschmer et al., 2018).

In this work, the characteristics of the vertical variation of wind speed are analysed within the limit of the surface boundary layer, where some of the most important variables are: friction velocity, momentum and energy fluxes, and surface roughness. Therefore, we can neglect the Coriolis parameter, baroclinity, wind shear, and entrainment processes near the top of the boundary layer. The effect of the wind speed vertical profile in the wind resource assessment at La Ventosa, Oaxaca, Mexico. This region is of special interest. It concentrates the greatest wind potential in Oaxaca due to the strong mountain gap wind travelling through the Chivela Pass into the eastern Pacific coast in southern Mexico, most commonly between October and February (Hong et al., 2018). We explore if the Monin–Obukhov similarity theory is suitable to describe the vertical wind speed within the surface boundary layer at the test site. Moreover, it is analysed the default International Electrotechnical Commission (IEC) (IEC61400-1, 2005; IEC61400-2, 2013) standard value and variable power-law method.

Furthermore, we study how the vertical wind profile influences wind power production in the rotor swept area using the rotor equivalent wind speed definition (Wagner et al., 2011; Commission et al., 2005), which it takes into account that the wind speed at hub height does not represent the wind speed at the lowest and upper part of a large-scale wind turbine rotor (European Wind Energy Association and others, 2012; Wharton and Lundquist, 2012).

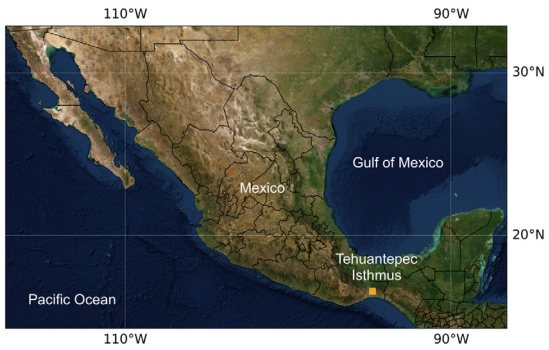

(a) The location of the measurement site at the Tehuantepec Isthmus, Oaxaca, Mexico (16°32′40.8″ N, 94°57′09.0″ W) is shown by the orange square.

(b) Geo-localization of the AEM mast in the CERTE laboratory.

Fig. 1. (a) Location of the measurement site at the Isthmus of Tehuantepec, and (b) location of the AEM mast at the CERTE laboratory.

2. Data and methods

2.1. Measurement site

Mexico has a large and diverse renewable energy resource such as solar, wind, biomass, hydropower and geothermal. Among these, wind power is one of the most efficient and developed energy sources (Thakur et al., 2016). Mexico is the second-largest wind power producer in Latin America after Brazil, with a total installed capacity of 6789 MW at the end of 2020 (GWEC, Global Wind Energy Council, 2020).

Figs. 1(a) and 1(b) show the measurement site at La Ventosa, Oaxaca in the Tehuantepec Isthmus region, Mexico. La Ventosa concentrates 33% of the country's total installed capacity of the country (GWEC, Global Wind Energy Council, 2020). The windy Isthmus region is relatively flat, and the maximum resource generally occurs from late morning to afternoon. However, during the windiest months (November through February), the wind resource is sometimes slightly greater at night than during the day (Lopez-Villalobos et al., 2021; Elliott et al., 2003). This suggests that effects related to the boundary layer stability are at play during these months.

Near the test site, to the north, is La Ventosa city, and there are some wind farms surrounding the area. La Ventosa region has been the subject of several studies to determine the region's wind characteristics (Cadenas and Rivera, 2007; Jaramillo and Borja, 2004; Lopez-Villalobos et al., 2018, 2021). It is known that the frequency distribution of wind speed is bimodal, a feature that is closely related to the wind direction, with northerly winter winds being stronger (Romero-Centeno et al., 2003; Jaramillo and Borja, 2004). Furthermore, the reliability of the IEC61400's Normal Turbulence Model (NTM) for fatigue load design parameter (IEC61400-1, 2005; IEC61400-2, 2013) is proven to be unsuitable for the location due to present greater wind dispersion than the standard NTM reported (Lopez-Villalobos et al., 2018). A power spectrum analysis has been conducted in the region and found a spectral gap and a microscale region with similar variance, allowing the use of mean-times from 6 h to 1 min with no significant difference in the wind resource assessment results (Lopez-Villalobos et al., 2021).

2.2. Data processing

Measurements from an 80 m high anemometric mast located at the Centro Regional de Tecnología Eólica (CERTE, shown in Fig. 1(b)) in La Ventosa, Oaxaca (16°32′49.27″ N, 94°57′20.83″ W) were used. These data were provided by the Mexican Wind Atlas (AEM, by its acronym in Spanish), funded by the United Nations Development Programme Global Environmental Finance (UNDP-GEF) unit and implemented by Mexico's Instituto Nacional de Electricidad *y* Energías Limpias (INEEL). The horizontal wind speed and direction were measured at four heights: 80, 60, 40, and 20 m. In addition, measurements of air temperature at 15 and 40 m and pressure at 15 m were used. The data were averaged and saved every 10 min from december 1st of 2017 to december 1st of 2018.

Virtual and potential air temperature need to be estimated to carry out the atmospheric stability analysis from the AEM measurements. Therefore, the potential air temperature was estimated as $\theta = T(P_0/P)^{0.286}$, where $P_0 = 1000$ hPa is the atmospheric reference pressure, and P is the air pressure. The virtual potential air temperature was calculated as $\theta_v = \theta(1+0.6r)$, where r is the mixing ratio for unsaturated air. We calculated r using the relative humidity measured at the site, following the methodology described in Bolton (1980).

To extrapolate the wind speed vertically, we need to estimate the Richardson stability parameter, which is proportional to the height above the surface at which buoyant factors dominate over mechanical production of turbulence (Stull, 1988). Virtual potential air temperature is analogous to potential air temperature in the sense that they both remove the air temperature variation caused by pressure changes of an air parcel. Thus, we can compare air parcels at different elevations to determine which one is warmer or cooler when brought to the same height. It is also a helpful quantity because it takes moisture and air temperature into account when considering buoyancy and stability. So, we can analyse virtual air temperature variations instead of variations in density.

2.3. Vertical velocity profile and atmospheric stability

The variation of wind speed with height in the surface boundary layer is typically well described by a logarithmic relationship between surface stress (represented by the friction velocity, u_*) and surface roughness (represented by the aerodynamic roughness length, z_0). In the present work, the wind profile in non-neutral conditions, which integrates the Businger–Dyer relationships (Dyer, 1974; Businger et al., 1971), is estimated by

$$u = \left(\frac{u_*}{k}\right)\left[\ln\left(\frac{(z-d)}{z_0}\right) - \psi_m\left(\zeta_m\right)\right], \tag{1}$$

where k is the Von Karman constant (0.4), z is the vertical height, d is the zero plane displacement ($d = 0$ for bare soil surfaces (Garratt and Hicks, 1973) which is the case in the present study), z_0 is the surface roughness, u_* is the friction velocity, and ψ_m is a stability correction function which depends on the ratio $\zeta_m = (z-d)/L$, where L is the Obukhov length. The friction velocity is defined as $u_* = k\Delta U/\phi_m \ln(z_2/z_1)$, where ϕ_m is a Monin–Obukhov stability correction function also known as the dimensionless wind shear, z_2 and z_1 correspond to the heights of available measurements (in our case 40 and 15 m, respectively), and ΔU is the change in horizontal wind speed at these heights.

The Richardson number, $Ri_m = \frac{g\Delta\theta_v z_m}{T_0(\Delta U)^2}\ln\left(\frac{z_2}{z_1}\right)$, serves as an indicator of forced and free convection instability mechanisms (Arya, 2001), where $\Delta\theta_v$ is the virtual potential air temperature difference at two different heights, T_0 corresponds to the absolute air temperature at height z_1, g is the acceleration due to gravity, $z_m = (z_2 z_1)^{1/2}$ is the geometric mean height. Richardson number is useful to classify the atmosphere in the surface layer as unstable, neutral, and stable. Negative Ri_m values indicate that convection predominates, winds are weak, and a strong vertical motion is characteristic of an unstable atmosphere, while for positive values lower than 0.2, the atmosphere is stable (Arya, 2001; Stull, 1988).

The ϕ_m and $\psi_m(\zeta_m)$ stability functions have been empirically determined in various studies (Businger et al., 1971; Deardorff, 1972; Nickerson and Smiley, 1975). The corresponding value of the stability parameter $\zeta_m = z_m/L$ can be determined from (Zilitinkevich and Calanca, 2000; Newman and Klein, 2014)

$$\zeta_m = \begin{cases} \dfrac{Ri_m}{1-\beta Ri_m}, & 0 \le Ri_m < 0.2, \\ Ri_m, & Ri_m < 0. \end{cases} \tag{2}$$

Knowing ζ_m, ϕ_m is determined as

$$\phi_m = \begin{cases} (1-\gamma\zeta_m)^{-1/4}, & \zeta_m < 0, \\ (1+\beta\zeta_m), & \zeta_m \ge 0. \end{cases} \tag{3}$$

and $\psi_m(\zeta_m)$ is determined as

$$\psi_m(\zeta_m) = \begin{cases} -\beta\zeta_m, & \zeta_m > 0, \\ \ln\left[\left(\dfrac{1+x^2}{2}\right)\left(\dfrac{1+x}{2}\right)^2\right] - 2\tan^{-1}(x) & \\ \quad + \dfrac{\pi}{2}, & \zeta_m < 0, \end{cases} \tag{4}$$

where $x = (1-\gamma\zeta_m)^{1/4}$. In the Eqs. (2) to (4), γ and β are coefficients determined using nonlinear least-squares best fits applied to observations (Dyer and Hicks, 1970; Dyer, 1974; Högström, 1996; Maronga and Reuder, 2017). The values of these coefficients have been extensively debated in the past literature. Although 4.7 is commonly accepted for β (Irwin, 1979; Businger et al., 1971; Deardorff, 1972; Zoumakis and Kelessis, 1991), a value of 5 is also frequently used (Zannetti, 2013; Garratt and Hicks, 1990). For γ, a value of 16 was proposed (Garratt and Hicks, 1990; Holtslag, 1984), although 15 is also recommended (Businger et al., 1971; Deardorff, 1972; Nickerson and Smiley, 1975). However, we note that those equations are not the only possible formulations, and we refer the reader to Optis et al. (2016) and Foken (2006) to discuss alternative forms of these relationships. In the current work, the values of β = 5 and γ = 15 were set.

Despite the limitations of the logarithmic wind speed profile in stable conditions, it is still frequently used under these conditions for wind power resource assessment and forecasting at altitudes within a few hundred metres of the surface. Over the last two decades, it has been used extensively in wind power meteorology (Petersen et al., 1998; Burton et al., 2011; Lange and Focken, 2006; Motta et al., 2005; Van den Berg, 2008; Emeis, 2010, 2018; Giebel et al., 2011; Drechsel et al., 2012). For wind power forecasting, in particular, the logarithmic wind speed profile has been used to interpolate wind speeds between two numerical weather prediction model levels to hub height, extrapolate observed wind speeds to hub height, or extrapolate the geostrophic winds to hub height using the friction velocity computed from the geostrophic drag law (Tennekes, 1973).

An alternative approach is given by the power-law method. This is a well-known engineering method commonly used to vertically extrapolate wind speed. The equation is written as $u(z) = u_r\,(z/z_r)^{\alpha}$ where α is the wind shear exponent, commonly assumed to be $\alpha = 1/7 \simeq 0.143$ for neutral atmospheric stability as recommended by the IEC61400 standard (IEC61400-2, 2013), u_r and z_r are the reference wind speed and height, respectively, and z is the height to which wind speed is to be extrapolated. A fixed wind shear coefficient may, in some cases, result in under or overestimation of wind speeds and wind power production (Fırtın et al., 2011; Rehman et al., 2013; Schwartz and Elliott, 2006). There are efforts to modify the standard power-law methodology to improve the prediction of wind speeds at higher heights; however, in many cases, a fixed wind shear coefficient is used based on long-term average time series wind data (Corscadden et al., 2016; Gualtieri, 2016). A constant wind shear coefficient is a factor that contributes to increasing uncertainty in wind speed extrapolation whilst using a variable wind shear coefficient provides a more accurate estimate of wind speed at hub height (Gualtieri, 2016; Đurišić and Mikulović, 2012).

2.4. Wind power resource assessment

In wind power projects, it is essential to determine the wind energy potential of a specific site. Then, the wind power production is estimated using a ten-minute wind speed time series and a wind turbine power curve. In this study, the Vestas V90-2MW wind turbine power curve was used (Fig. 2), corresponding to a

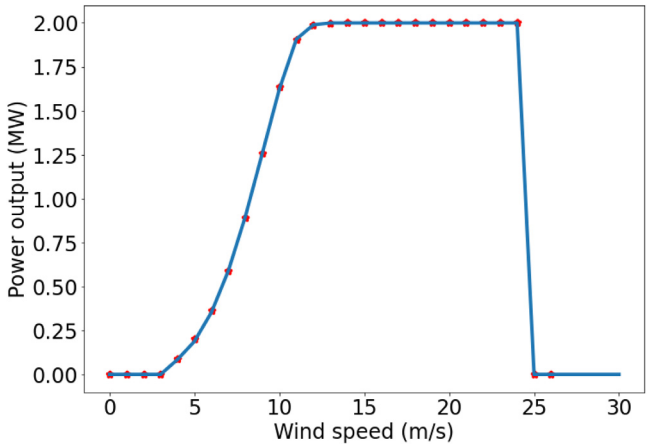

Fig. 2. Power curve of the Vestas90 with a nominal power of 2 MW, diameter of 90 m, 3 blades and pitch power control. The red symbols are the manufacturer's power curve data, and the solid blue line is a curve fitting to the data.

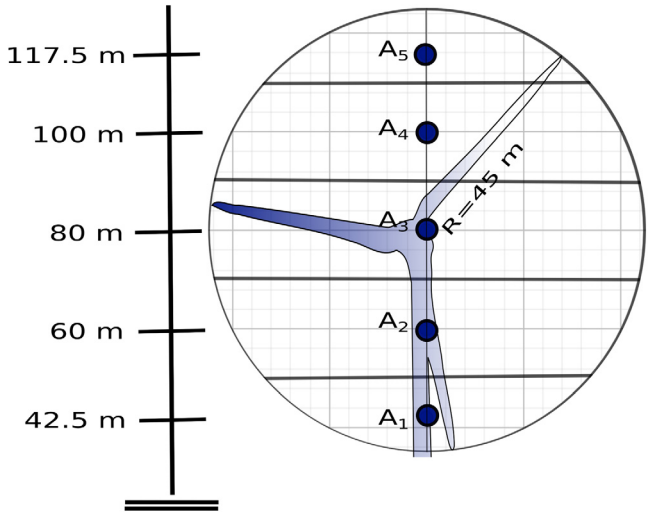

Fig. 3. Illustration of determination of equivalent rotor wind speed over the rotor swept area divided into four segments corresponding to the four heights AEM measurements. Each wind speed is assumed to be constant in each segment.
Source: Adapted from Wagner et al. (2011).

three-bladed upwind horizontal axis wind turbine. The V90-2MW has a rotor diameter of 90 m, with rotor blades of 44 m long, and a hub height of 80 m above surface level (Vestas, 2015). It starts producing electric power at a wind speed of 3 m/s, reaching its nominal power output of 2 MW at 13.5 m/s, and the survival wind speed is 25 m/s, which is the power production cutoff wind speed (pitch power control).

The mean energy production of a wind turbine, $\overline{P_T}$, for a given time series with N data points, is defined as (Manwell et al., 2010):

$$\overline{P_T} = \frac{1}{N}\sum_{j=1}^{N} P_T(V_{eq}(t_j)), \tag{5}$$

where P_T is the wind turbine power production as a function of the rotor equivalent wind speed, $V_{eq}(t) \geq 0$. The rotor equivalent wind speed is the wind speed corresponding to the kinetic energy flux through the swept rotor area, when accounting for the vertical shear (Wagner et al., 2014). The simplest model for V_{eq} accounts for only the wind speed shear and does so by dividing the turbine's rotor disk into discrete vertical layers, as follows:

$$V_{eq}(t) = \left(\sum_i u_i^3(t)\frac{A_i}{A}\right)^{1/3}, \tag{6}$$

where A represents the area swept out by the rotor disk, A_i the area of a discretized section of the rotor disk (as shown in Fig. 3), and u_i is the wind speed measured in the given section. The section area ratios are defined as follows: $A_1/A = 0.125$, $A_2/A = 0.25$, $A_3/A = 0.25$, $A_4/A = 0.25$, and $A_5/A = 0.125$. From Fig. 3, the hub height is 80 m above ground level, and the wind turbine rotor radius is 45 m.

3. Results

3.1. Atmospheric stability

The vertical variation of the hourly mean virtual potential air temperature and its spread (25 and 75th percentile values) throughout the year is shown in Fig. 4. It is important to mention that the local time (LT) corresponds to GMT-6 and we will use LT instead. Throughout the year, the mean virtual air temperature starts increasing around 07:00 h, reaching a maximum value around 14:00–15:00 h, and then it starts to decrease slowly, showing a net radiative loss of energy from the surface during night time. The seasonal behaviour of the hourly virtual potential air temperature shows higher values during spring and summer (Figs. 4(a), 4(b)). It is interesting to note the variation of the spread throughout the year, with higher spread during autumn and winter than during summer. Moreover, Fig. 4 shows, consistently for all seasons, a slight increase of temperature with height occurring mainly between 20:00 h to 06:00 h, called inversion. The most common inversion is radiational inversion, which happens due to the radiational cooling of the earth's surface. Because of the longwave radiation to space, the earth is cooled at night. The inversion is maximized on clear nights with light wind and dry air, but it generally erodes rapidly once daytime heating warms the lower planetary boundary layer.

Fig. 5 shows the seasonal differences of the hourly mean virtual potential air temperature at both heights, which we define as $\partial\theta_v/\partial z \approx \Delta\theta/\Delta z = (\theta(z2) - \theta(z1))/(z_2 - z_1)$, where $z_2 > z_1$. The criteria for static stability is then based on the sign of this gradient (Arya, 2001). If $\partial\theta_v/\partial z > 0$ corresponds to a stable stratification, otherwise is unstable. The greater differences are found in spring from 00:00 to 06:00 h during stable condition and in summer from 19:00 to 23:00 h.

Fig. 6 shows the hourly mean friction velocity values, which represent the intensity of the turbulent movement of the air masses on the surface due to the roughness present at the site. The general behaviour of the friction velocity shows a diurnal variability, similar to the potential air temperature, which is expected due to the forcing occurring in the atmospheric boundary layer by solar heating. u_* typically varies daily with low u_* during calm nights (calm winds) ($u_* = 0$) and high u_* during daytime (strong winds) ($u_* = 1$ m/s). Moderate wind values are often near $u_* = 0.5$ m/s, which might be related to moderate mean friction velocity values during the spring and summer (from 0.35 to 0.5 m/s). High mean friction velocity values (from 0.5 to 0.75 m/s) for the winter and autumn are related to high wind speed mean values. The maximum values are found during the winter season, reaching a maximum mean value of 0.75 m/s at 16:00 h, which coincides with an unstable thermal static atmosphere. We found a lower mean value during spring and summer, where the lowest wind speed values of the year are found, around 0.33 m/s. Furthermore, the highest dispersion (Vertical lines) is observed

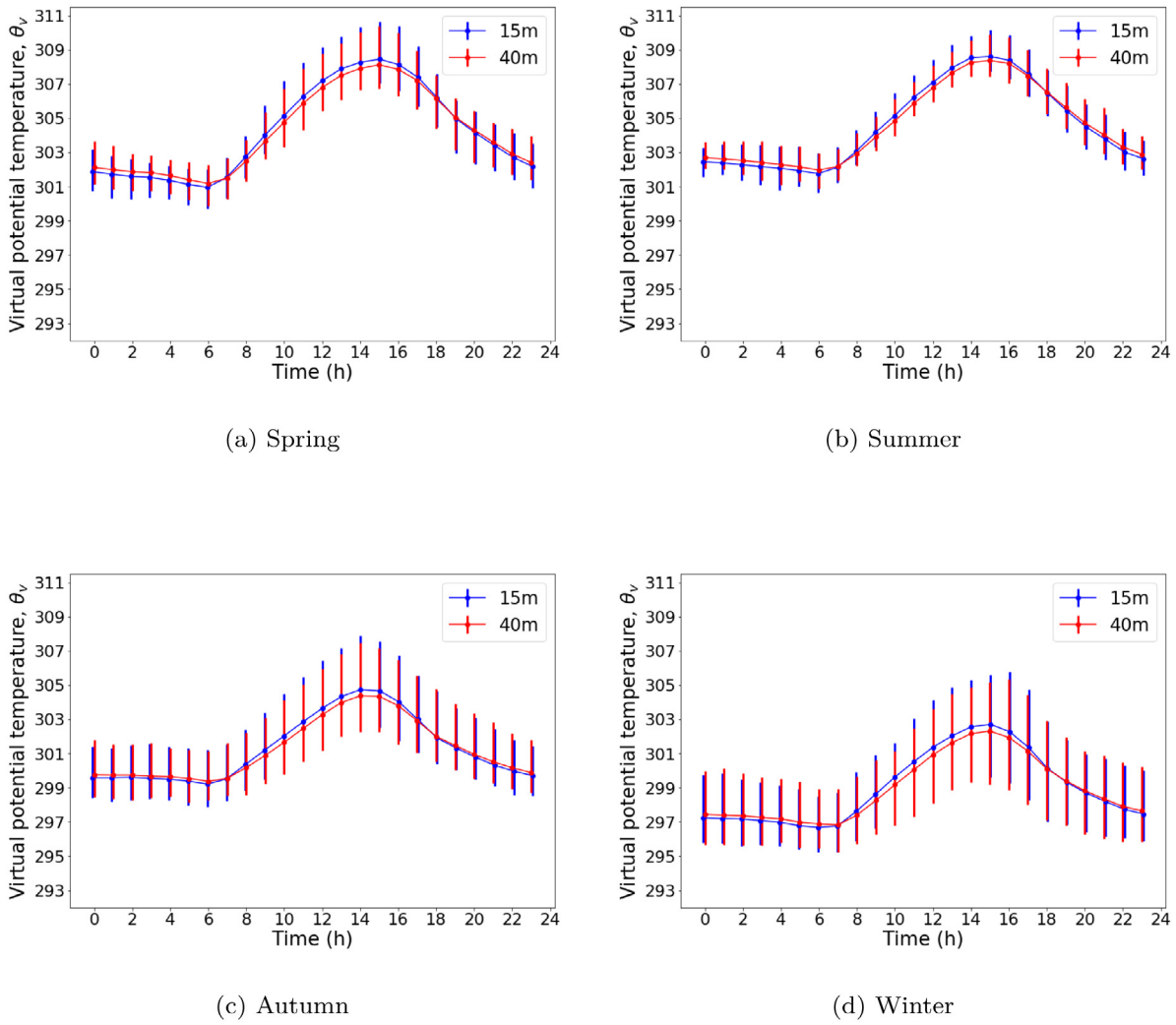

Fig. 4. Seasonal variation of the hourly mean virtual potential air temperature: (a) spring (March–May 2018); (b) summer (June–August 2018); (c) autumn (September–November 2018), and (d) winter (December 2017, January–February 2018), for 15 m and 40 m height. The vertical lines go from the 25th to 75th percentile. .

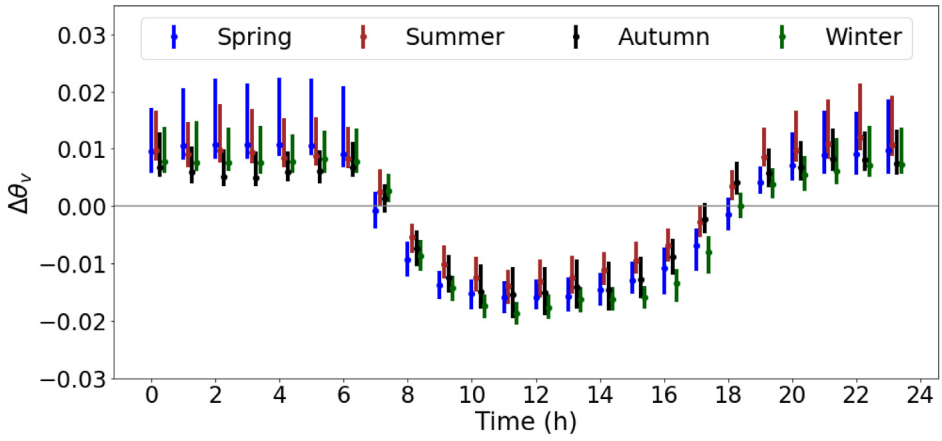

Fig. 5. Seasonal differences of the hourly mean virtual potential air temperatures between 40 and 15 m heights. The vertical lines go from the 25th to the 75th percentile.

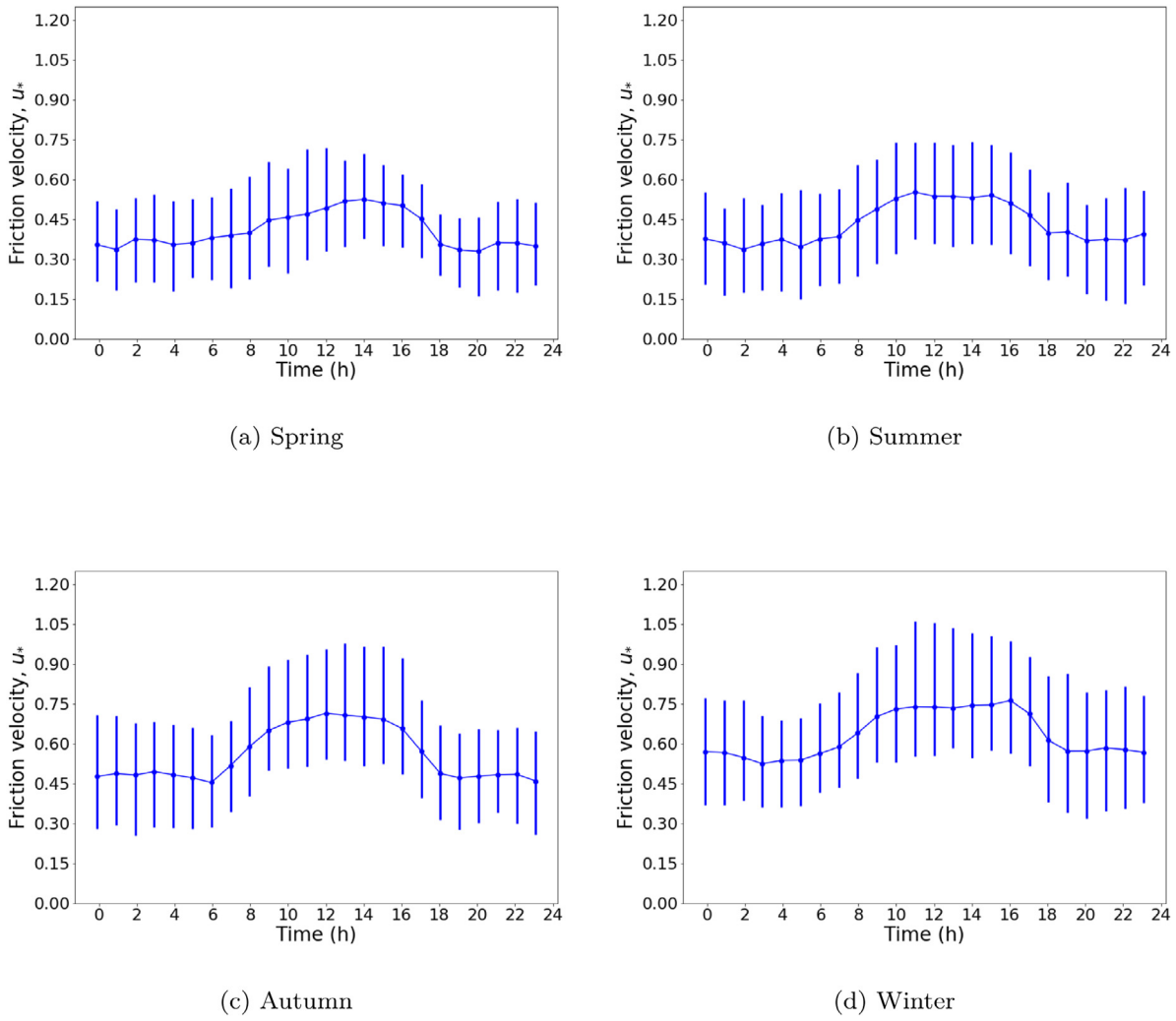

Fig. 6. Seasonal variation of the hourly mean friction velocity (m/s): (a) spring (March–May 2018); (b) summer (June–August 2018); (c) autumn (September–November 2018), and (d) winter (December 2017, January–February 2018) at $z_m = (z_2 z_1)^{1/2} = 24.5$ m above the surface. z_1 and z_2 correspond to 15 and 40 m, respectively. The vertical lines go from the 25th to the 75th percentile. .

in the winter and autumn seasons, which are the seasons with the highest wind speed shear. During the day, u_* varies from 0.63 to 0.97 m/s throughout the seasons, where the maximum value occurs in winter and the minimum in spring. During the night, it varies from 0.51 to 0.79 m/s, where the maximum occurs in winter and the minimum in spring.

Fig. 7 shows the hourly mean seasonal behaviour throughout the day of the ζ_m time series. The figure shows that there is a mixture of stable and unstable conditions; however, while the sun is heating the region's surface (08:00 h to 17:00 h), unstable conditions dominate. The atmosphere is mostly unstable in all seasons, around 70% of the time.

3.2. Wind profile adjustment

The seasonal behaviour of $\psi_m(\zeta_m)$ is displayed in Fig. 8. In general, it exhibits a diurnal pattern similar to ζ_m but with the opposite sign, so that under unstable conditions $\psi_m(\zeta_m)$ is positive while under stable conditions it is negative. Consequently, the velocity profiles in the surface layer are expected to become increasingly curvilinear as instability increases.

The wind shear exponent $\alpha = 1/7$ is recommended by the IEC61400 standard (IEC61400-2, 2013) for neutral atmospheric conditions with values higher (lower) than 1/7 indicating stable (unstable) conditions (Newman and Klein, 2014). We used the power-law equation, $U_z = U_r(Z_z/Z_r)^{\alpha}$, to estimate variable wind shear exponent as $\alpha = \ln(U_z/U_r)/\ln(Z_z/Z_r)$. Here, U_z and U_r are equal to the wind speed time series measured at Z_z = 80 m and Z_z = 20 m, respectively. Fig. 9 shows the seasonal variability of the hourly mean wind shear exponent. During the day, the mean α values range between 0.12 and 0.20 indicating almost neutral atmospheric conditions. During the night, the α values range between 0.20 to 0.25, which indicates stable atmospheric conditions.

Until now, we do not have information about the roughness length z_0, but we can estimate it using the known variables. We can estimate the variability of z_0 from data by obtaining seasonal roughness values. To estimate z_0, we use a least-square fitting to the AEM measurements. Table 1 shows the variability of z_0 ranging from 0.20 to 1.15 m, which is reported in the literature as a farmland terrain that matches the type of terrain of the site.

Table 1 summarizes the seasonal and diurnal mean values of u_*, $\psi_m(\zeta_m)$, z_0 and α. The latter, during day, is close to the IEC neutral atmospheric stability recommendation, but during night, is larger than recommendation, mostly during stable atmospheric conditions. These variables are used as input to vertically extrapolate the wind speed.

The seasonal wind speed profiles during the day and night are shown in Figs. 10 and 11, respectively. During the day, in

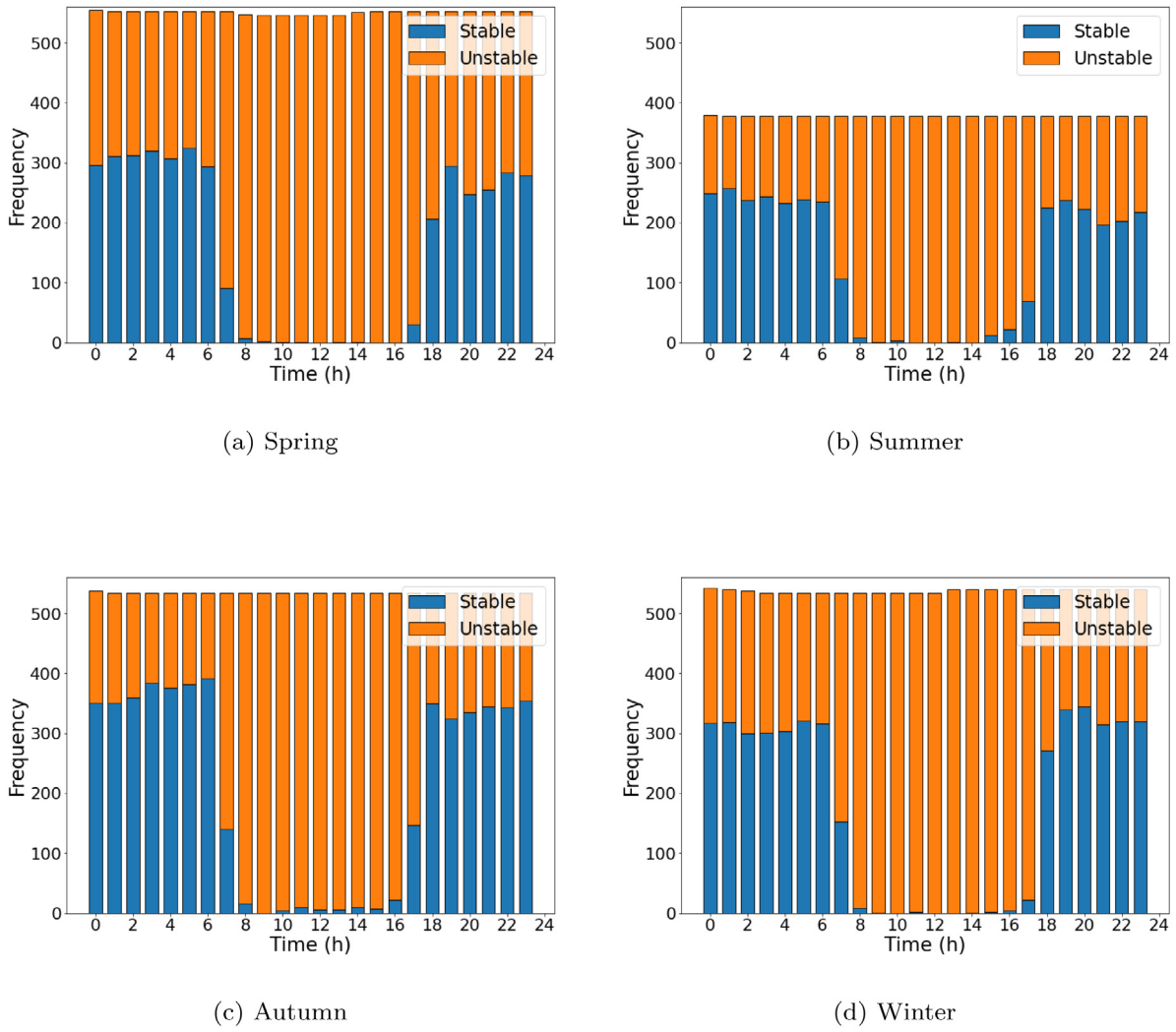

Fig. 7. Frequency distribution of hourly stability data by season: (7(a)) spring, (7(b)) summer, (7(c)) autumn, (7(d)) winter, based on the Obukhov length time series at $z_m = (z_2 z_1)^{1/2} = 24.5$ m above the surface. z_1 and z_2 correspond to 15 and 40 m, respectively. .

Table 1
Summary of the vertical profile variables used in the log-law and power law equations, according to the season of the year and daytime conditions.

Season	Variables	u_*	$\psi_m\ (\zeta_m)$	z_0	α
Spring	Daylight	0.63	0.78	0.20	0.14
	Night	0.51	−0.98	1.05	0.22
Summer	Daylight	0.68	0.43	0.30	0.15
	Night	0.52	−1.06	0.87	0.22
Autumn	Daylight	0.87	0.21	0.38	0.17
	Night	0.68	−1.45	1.15	0.22
Winter	Daylight	0.97	0.50	0.22	0.16
	Night	0.79	−0.45	0.38	0.21

Fig. 10, the mean values generally show a good fit, although, for autumn and winter seasons, the estimation using the default value ($\alpha = 1/7$) tends to deviate more from the mean values above 20 m height. In Fig. 11, the estimations obtained using the default wind shear exponent deviates from mean values during the stable atmospheric condition at night. Moreover, for the log-law model, the estimations deviate from the mean values at 20 and 80 m height. Additionally, the variable wind shear method predicts the tendency of the AEM mean values. Now, we will compare the wind speed profiling methods against the AEM measurements. We will use the index of agreement defined as $IOA = 1 - \frac{\sum_{i=1}^{n}(P_i - O_i)^2}{\sum_{i=1}^{n}(|P_i - \overline{O}| + |O_i - \overline{O}|)^2}$, which is a standardized measure of the degree of model prediction error and varies between 0 and 1. A value of 1 indicates a perfect match, and 0 indicates no agreement at all (Willmott, 1981). The IOA is shown in Table 2 of the power-law and log-law methods compared against AEM dataset. In the columns are shown, diurnally, the seasonal mean variable wind shear exponent and using a default value of 1/7. In general, there is a good general agreement with the AEM dataset. The log-law and the variable wind shear exponent power-law method has a IOA values closely 1.0. Moreover, the power-law adjustment using $\alpha = 1/7$ has a good agreement, but throughout the year nights show the lowest IOA values amongst all adjustment. The latter is because, during the night, the wind speed is greater than predicted by the model. We can say that stable atmospheric conditions is expected to present higher wind speed than neutral atmospheric conditions.

3.3. Effects of vertical wind shear in wind power production

In this section, we assess the influence of using the different wind speed extrapolation methods in the wind resource assessment for a whole year. Seasonal mean ψ_m value and seasonal u_*

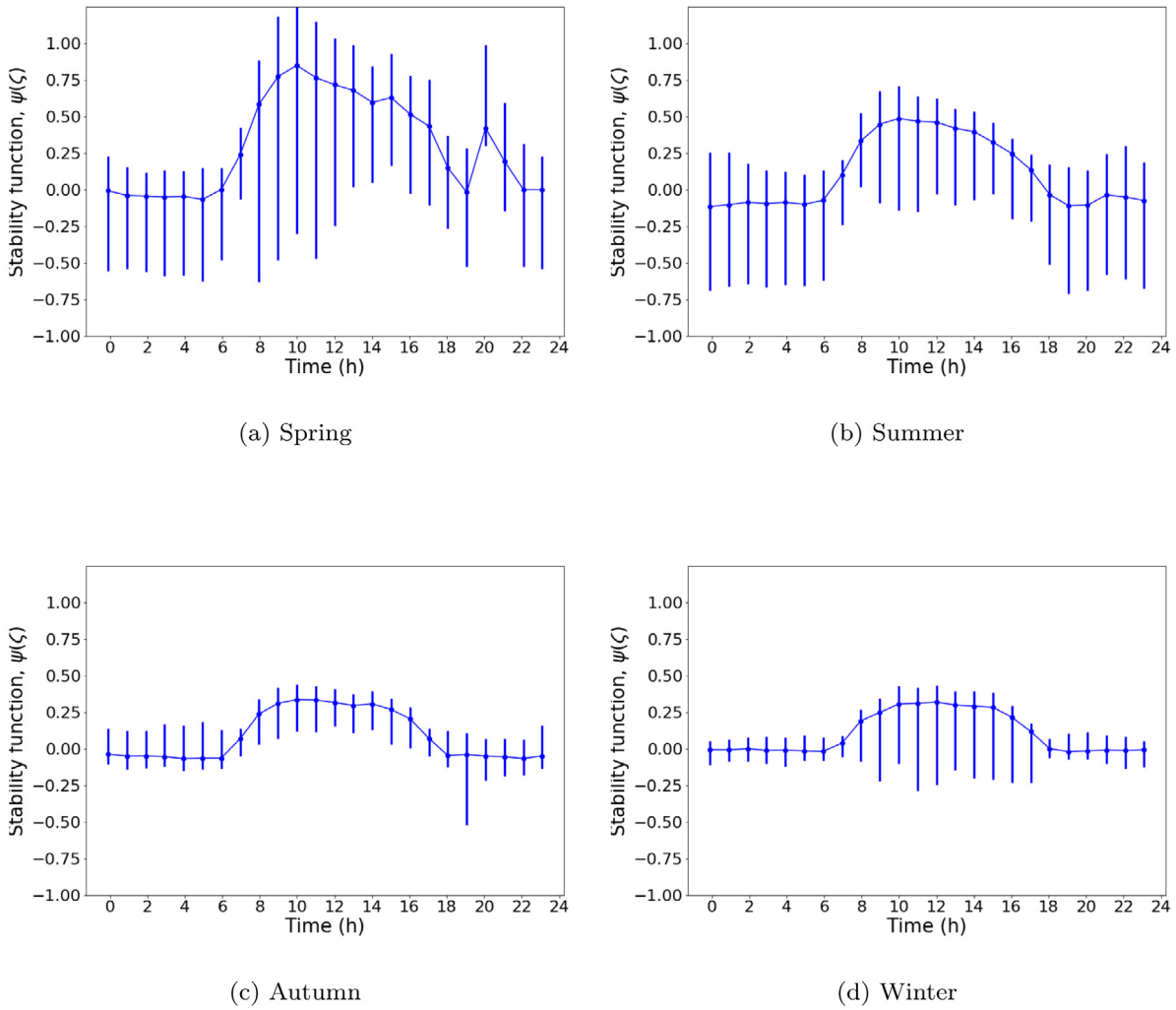

Fig. 8. Seasonal variation of the hourly mean stability function correction: (a) spring (March–May 2018); (b) summer (June–August 2018); (c) autumn (September–November 2018), and (d) winter (December 2017, January–February 2018) at $z_m = (z_2 z_1)^{1/2} = 24.5$ m above the surface. z_1 and z_2 correspond to 15 and 40 m, respectively. The vertical lines go from the 25th to 75th percentile. .

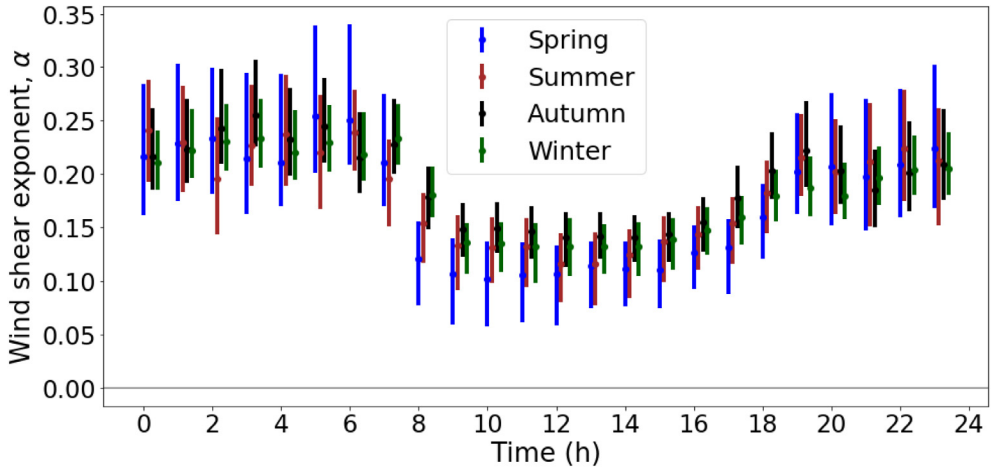

Fig. 9. Seasonal variation of the hourly mean wind shear exponent (α) between 80 and 20 m heights. The vertical lines go from the 25th to 75th percentile.

time series were used to calculate the wind power production (Eq. (5)). The reference value of 20 m of the AEM measurement was used as an input of the power-law (IEC standard and seasonal variable wind shear value) and log-law method to extrapolate to 42.5, 60, 80, 100 and 117.5 m.

Fig. 12 shows the mean power output $\overline{P_T(V_{eq})}$ using the equivalent wind speed determined from the log-law and power-law ($\alpha = 1/7$ and variable α) method. We will use the variable wind shear exponent method as a reference value because it has demonstrated good agreement against AEM measurements. In

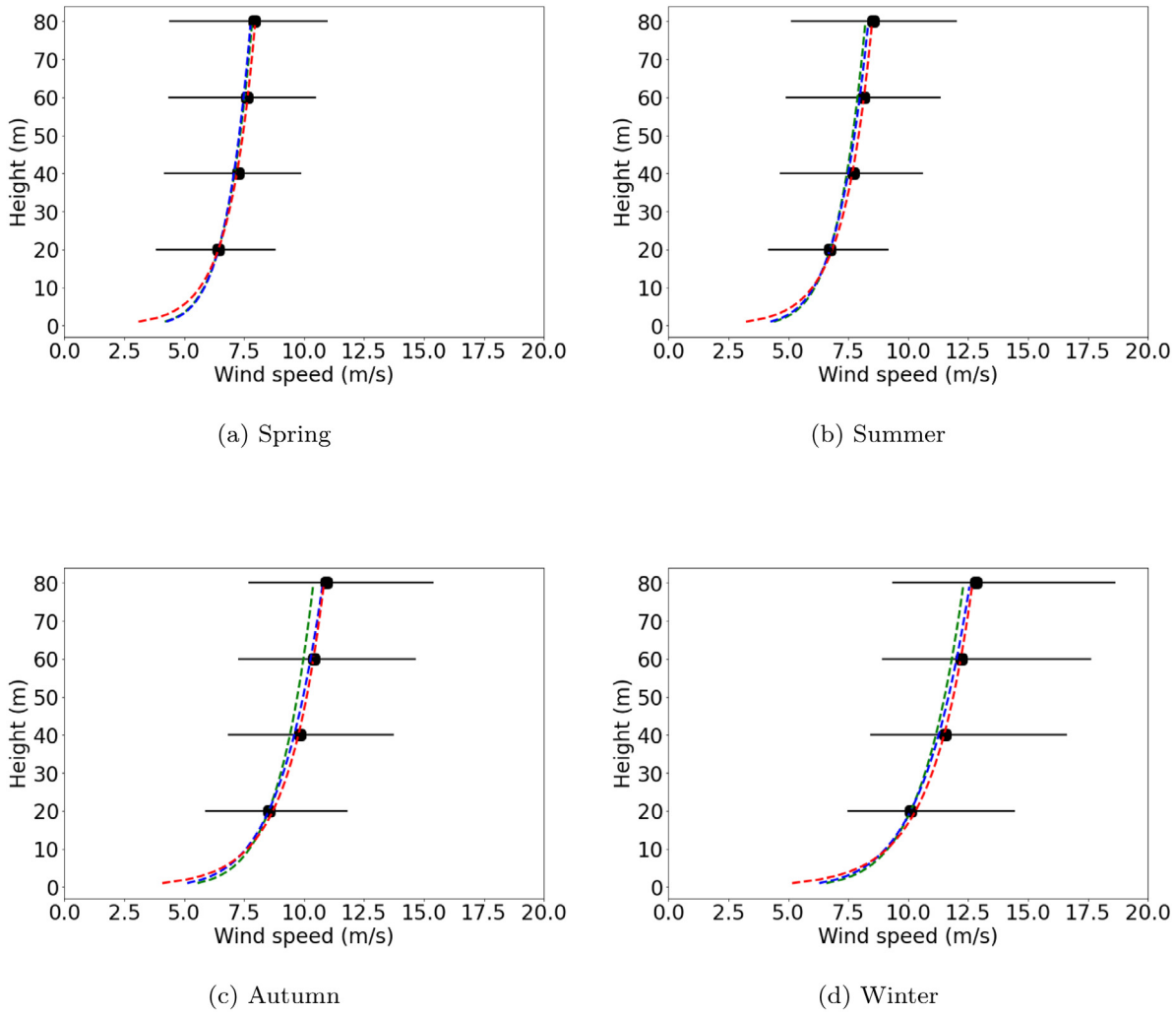

Fig. 10. Vertical wind speed profiles from different adjustments to the AEM measurements during daylight for (a) spring, (b) summer, (c) autumn, and (d) winter seasons. The blue dashed line (- - -) represents the profile estimated from the variable wind shear exponent of the power-law equation. The green dashed line (- - -) corresponds the profile estimated from the power-law considering $\alpha = 1/7$, which is the IEC61400 standard recommendation. The red dashed line (- - -) represents the profile obtained using the log-law equation. The black solid markers (—■—) represent the mean values from the AEM measurements, and error bars (horizontal lines) go from the 25th to the 75th percentile. (For interpretation of the references to colour in this figure legend, the reader is referred to the web version of this article.)

Table 2
Index of agreement of wind speed profiling adjustment methods: Power law (P.l), Log-law (L-l).

Season	Index of agreement (IOA)		
	P.l (variable)	P.l ($\alpha = 1/7$)	L-l
Spring day	0.98	0.99	0.99
Spring night	0.99	0.86	0.97
Summer day	0.98	0.96	0.99
Summer night	0.99	0.84	0.96
Autumn day	0.99	0.94	0.99
Autumn night	0.99	0.85	0.96
Winter day	0.99	0.96	0.99
Winter night	0.99	0.89	0.97

general, $\overline{P_T(V_{eq})}$ has a seasonal and diurnal dependency, reaching a maximum during daylight in winter. The $\alpha = 1/7$ under-predicts a maximum of 13% less mean power output during the night, although during winter and spring, where the α value is nearly 1/7, there is an over-prediction of 0.6% more mean power output. These results suggest that the IEC standard might be suitable for estimating wind resources if the only data available is wind speed at one height. However, the wind resource should be expected to be underestimated by about 12%.

Table 3 shows the mean power production using the AEM measurements at hub height (80 m) and using variable α and log-law method of extrapolation to the same height. The percentage error is greater for the log-law method, with an over-prediction of 9% for the extrapolated hub height wind speed. The method that best approached against AEM mean power prediction at hub height (80 m) was the variable wind shear exponent method, with a percentage error difference close to zero. Therefore, we recommend using the variable power-law method to estimate wind energy production based on the present results.

The power production difference between equivalent wind speed and hub height wind speed is assessed between AEM measurement at hub height (80 m) and the variable wind shear method. The latter is because the variable wind shear method has shown good agreement against AEM measurements. From Fig. 12 and Table 3 a maximum percentage error at night is shown during spring and summer seasons (1.6 and 1.3%, respectively) and a minimum error at daylight during winter season (0.2%). Although, there is, on average, 0.9% more power production if the wind shear is considered employing equivalent wind speed.

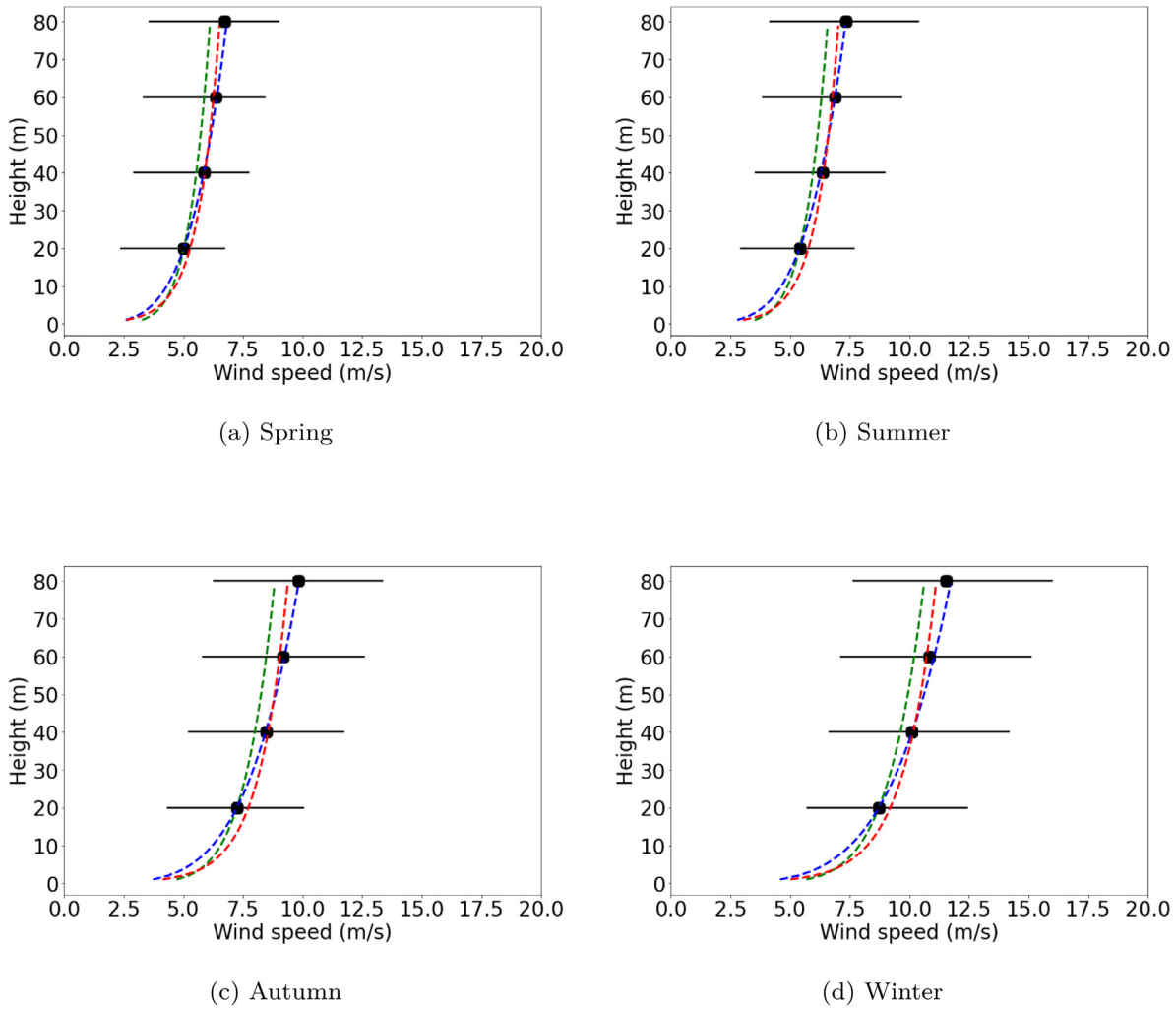

Fig. 11. Vertical wind speed profiles from different adjustments to the AEM measurements at night for: (a) spring, (b) summer, (c) autumn, and (d) winter seasons. The blue dashed line (- - -) represents the profile estimated from the variable wind shear exponent of the power-law equation. The green dashed line (- - -) corresponds the profile estimated from the power-law considering $\alpha = 1/7$, which is the IEC61400 standard recommendation. The red dashed line (- - -) represents the profile obtained using the log-law equation. The black solid markers (—■—) represent the mean values from the AEM measurements, and error bars (horizontal lines) go from the 25th to the 75th percentile. . (For interpretation of the references to colour in this figure legend, the reader is referred to the web version of this article.)

Table 3
Seasonal mean power output (P_T) at hub-height (80 m) of the AEM measurement, power-law(IEC & variable) and Log-law wind speed extrapolation method.

Season	Day			Night		
	P_T (MW)			P_T (MW)		
	Dynamic α	Log-law	AEM	Dynamic α	Log-law	AEM
Spring	0.898	0.960	0.898	0.698	0.693	0.698
Summer	1.049	1.070	1.049	0.833	0.811	0.833
Autumn	1.343	1.336	1.343	1.203	1.135	1.203
Winter	1.467	1.497	1467	1.379	1.339	1.379

The latter indicates no influence of the vertical wind speed variation within and on top (up to 117.5 m) the surface boundary layer on the mean power production. The ratio of the rotor diameter and the hub height is almost 1.12. The wind shear exponent mean values are 0.14 and 0.22, which confirms the conclusions reported in Van Sark et al. (2019), although the influence is dependent on the rotor size and hub height; therefore, it is necessary to analyse with other wind turbine power curves, and wind turbine measured power output.

If wind speed data is available at more than one height, the variable α method is recommended for wind resource assessment. However, if there is the air temperature and relative humidity data, the log-law model would give more information about the vertical wind profile within the surface boundary layer, which is useful for estimating wind turbine aerodynamic performance.

4. Summary and conclusion

This paper analyzes the effect of the vertical wind speed profile in the surface boundary layer on the mean power production of a horizontal axis wind turbine for La Ventosa, Oaxaca, in Mexico. Two of the most widely used vertical wind speed extrapolation methods for wind resource assessment, the power-law and log-law methods, were compared against wind speed data available in the AEM. For the power-law method, a constant value of the shear exponent, $\alpha = 1/7$, and a variable α were used. The log-law model and the power-law method using a variable α yielded IOA values close to 1.0, while good agreement was obtained for $\alpha = 1/7$. However, with $\alpha = 1/7$, the lowest IOA values were obtained among all the adjustments throughout the year-nights.

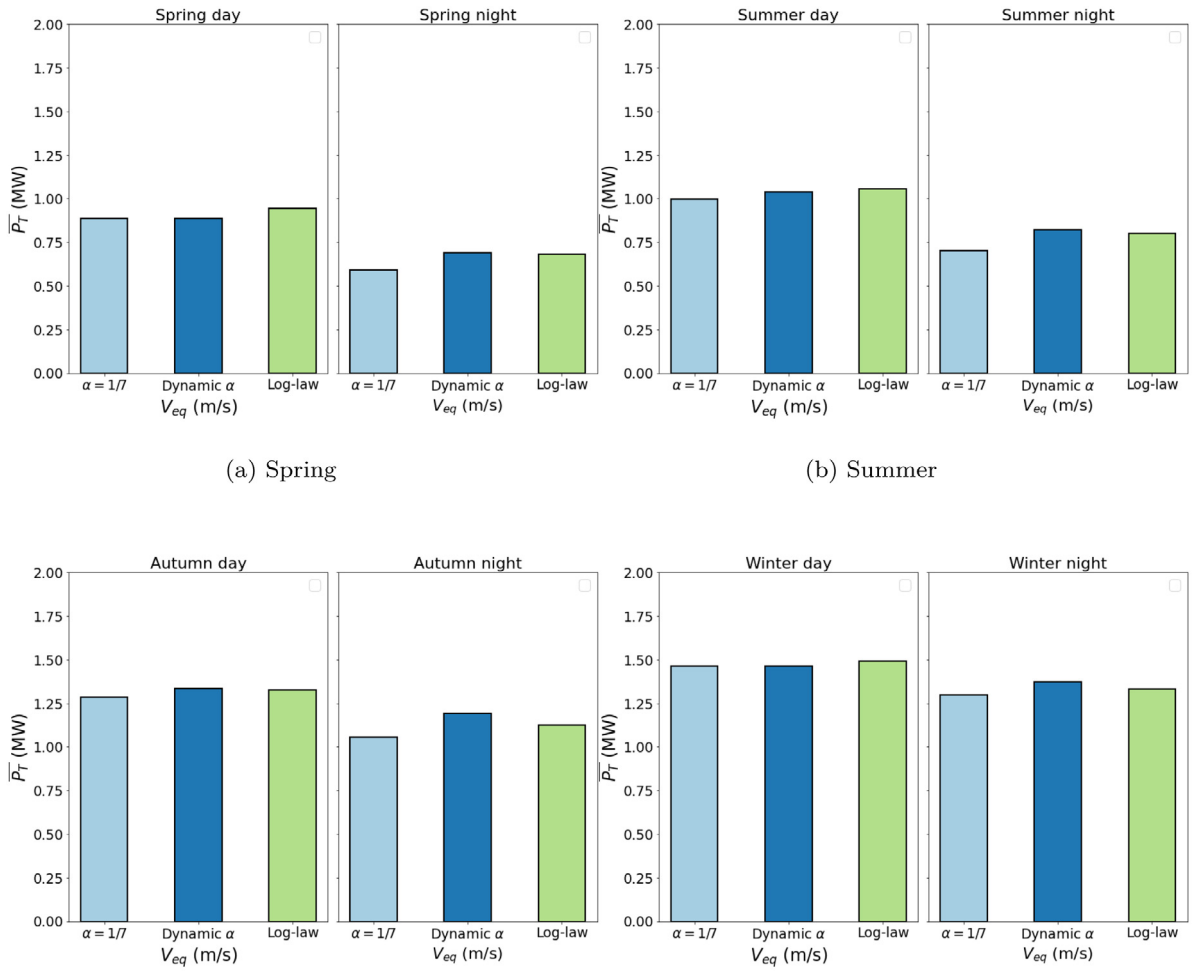

(a) Spring (b) Summer

(c) Autumn (d) Winter

Fig. 12. Mean power production of the Vestas90 using equivalent wind speed definition from AEM measurements and wind speed profiling methods. .

A comparison was made between the mean power production using the AEM measurements at 80 m, which corresponds to the Vestas90 wind turbine hub height, against that obtained by extrapolating the wind speed at the same hub height using the power-law method with variable α and the log-law model. The percentage error is greater when using the log-law model, with an overestimation of 9%. The method that best approximated the estimation of the mean power from the AEM data at 80 m was the power-law method using a variable α, with a percentage error close to zero.

Mean power output was estimated by the equivalent wind speed equation using available AEM measurements. The 20 m reference value of the AEM measurements was used for the power-law method ($\alpha = 1/7$ and variable α) and the log-law model to extrapolate to 42.5, 60, 80, 100, and 117.5 m. Variable α was used as reference value because it was in better agreement with the AEM measurements. With $\alpha = 1/7$, the average maximum power during the night is underestimated by 13%. However, during winter and spring, when the value of α is almost 1/7, there is an overprediction of 0.6% in mean power output.

We evaluated the effect of the vertical wind speed profile on the wind resource assessment by calculating the difference in mean power production using the equivalent wind speed and the wind speed at 80 m height. We found a minimum difference of 1.3%, indicating that the vertical variation of wind speed within and above (up to 117.5 m) the surface boundary layer does not influence the average power output for a wind turbine with a diameter of 90 m and a hub height of 80 m.

As a final comment, if wind speed data is available at more than one height, the α variable method is recommended for wind resource assessment. However, if complementary data, including air temperature and relative humidity, are available, the log-law method, specifically the similarity method, could provide more information about the state of the atmosphere, which is useful for aerodynamic performance of wind turbines.

CRediT authorship contribution statement

C.A. Lopez-Villalobos: Conceptualization, Methodology, Formal analysis, Investigation, Data curation, Visualization, Writing – original draft. **O. Martínez-Alvarado:** Writing – review & editing. **O. Rodriguez-Hernandez:** Writing – review & editing. **R. Romero-Centeno:** Conceptualization, Methodology, Writing – review & editing.

Declaration of competing interest

The authors declare that they have no known competing financial interests or personal relationships that could have appeared to influence the work reported in this paper.

Acknowledgements

This work was supported by a postdoctoral fellowship (DGAPA-UNAM) to C.A. Lopez Villalobos. The authors would like to thank the Universidad Nacional Autónoma de México (UNAM) for the support provided to carry out this work through PAPIIT project IN110721. O Martínez-Alvarado was supported by the National Centre for Atmospheric Science ODA national capability program ACREW (NE/R000034/1), which is supported by the UK's Natural Environment Research Council (NERC) and the Global Challenges Research Fund (GCRF). The contributions by O. Rodriguez-Hernandez were supported by project 272063, "Strengthening of the field of Wind Energy in the Doctoral Program in Engineering Field of Knowledge in Energy based in the Instituto de Energías Renovables of the UNAM"; call, Institutional Strengthening for Energy Sustainability; and fund, CONACYT-SENER-Sustentabilidad Energética for supporting the development of this research work.

References

Alfredsson, P.H., Segalini, A., 2017. Introduction wind farms in complex terrains: an introduction.

Archer, C.L., Jacobson, M.Z., 2003. Spatial and temporal distributions of US winds and wind power at 80 m derived from measurements. J. Geophys. Res.: Atmos. 108 (D9).

Arya, P.S., 2001. Introduction to Micrometeorology. Elsevier.

Van den Berg, G., 2008. Wind turbine power and sound in relation to atmospheric stability. Wind Energy Int. J. Progress Appl. Wind Power Convers. Technol. 11 (2), 151–169.

Bolton, D., 1980. The computation of equivalent potential temperature. Mon. Weather Rev. 108 (7), 1046–1053.

Burton, T., Jenkins, N., Sharpe, D., Bossanyi, E., 2011. Wind Energy Handbook. John Wiley & Sons.

Businger, J.A., Wyngaard, J.C., Izumi, Y., Bradley, E.F., 1971. Flux-profile relationships in the atmospheric surface layer. J. Atmosph. Sci. 28 (2), 181–189.

Cadenas, E., Rivera, W., 2007. Wind speed forecasting in the south coast of oaxaca, Mexico. Renew. Energy 32 (12), 2116–2128. http://dx.doi.org/10.1016/j.renene.2006.10.005.

Chanprasert, W., Sharma, R., Cater, J., Norris, S., 2020. Seasonal variability of offshore wind turbine wakes.

Commission, I.E., et al., 2005. Wind turbines-part 12-1: Power performance measurements of electricity producing wind turbines. In: IEC 61400-12-1.

Corscadden, K.W., Thomson, A., Yoonesi, B., McNutt, J., 2016. The impact of variable wind shear coefficients on risk reduction of wind energy projects. Int. Scholarly Res. Not. 2016.

Deardorff, J.W., 1972. Parameterization of the planetary boundary layer for use in general circulation models. Mon. Weather Rev. 100 (2), 93–106.

Donnou, H.E., Akpo, A.B., Kouchadé, C.A., Kounouhewa, B.B., Houngue, G.H., Nonfodji, G.F., Djossou, J., 2019. Vertical profile of wind diurnal cycle in the surface boundary layer over the coast of cotonou, benin, under a convective atmosphere. Adv. Meteorol. 2019.

Drechsel, S., Mayr, G.J., Messner, J.W., Stauffer, R., 2012. Wind speeds at heights crucial for wind energy: measurements and verification of forecasts. J. Appl. Meteorol. Climatol. 51 (9), 1602–1617.

Du, B., Ge, M., Zeng, C., Cui, G., Liu, Y., 2021. Influence of atmospheric stability on wind-turbine wakes with a certain hub-height turbulence intensity. Phys. Fluids 33 (5), 055111.

Dyer, A., 1974. A review of flux-profile relationships. Bound.-Lay. Meteorol. 7 (3), 363–372.

Dyer, A., Hicks, B., 1970. Flux-gradient relationships in the constant flux layer. Q. J. R. Meteorol. Soc. 96 (410), 715–721.

Elliott, D., Holladay, C., Barchet, W., Foote, H., Sandusky, W., 1987. Wind energy resource atlas of the United States. NASA STI/Recon Technical Report N 87, p. 24819.

Elliott, D., Schwartz, M., Scott, G., Haymes, S., Heimiller, D., George, R., 2003. Wind energy resource atlas of Oaxaca. Tech. rep., National Renewable Energy Lab.(NREL), Golden, CO (United States).

Emeis, S., 2010. A simple analytical wind park model considering atmospheric stability. Wind Energy 13 (5), 459–469.

Emeis, S., 2018. Wind Energy Meteorology: Atmospheric Physics for Wind Power Generation. Springer.

European Wind Energy Association and others, 2012. Wind Energy-the Facts: A Guide to the Technology, Economics and Future of Wind Power. Routledge.

Fırtın, E., Güler, O., Akdağ, S.A., 2011. Investigation of wind shear coefficients and their effect on electrical energy generation. Appl. Energy 88 (11), 4097–4105.

Foken, T., 2006. 50 Years of the monin–obukhov similarity theory. Bound.-Lay. Meteorol. 119 (3), 431–447.

Garratt, J., Hicks, B., 1973. Momentum, heat and water vapour transfer to and from natural and artificial surfaces. Q. J. R. Meteorol. Soc. 99 (422), 680–687.

Garratt, J., Hicks, B., 1990. Micrometeorological and PBL experiments in Australia. Bound.-Lay. Meteorol. 50 (1), 11–29.

Giebel, G., Draxl, C., Brownsword, R., Kariniotakis, G., Denhard, M., 2011. The state-of-the-art in short-term prediction of wind power. A literature overview.

Gormo, V.G., Kidmo, D.K., Ngoussandou, B.P., Bogno, B., Raidandi, D., Aillerie, M., 2021. Wind power as an alternative to sustain the energy needs in Garoua and Guider, North Region of Cameroon. Energy Rep. 7, 814–829.

Gualtieri, G., 2016. Atmospheric stability varying wind shear coefficients to improve wind resource extrapolation: A temporal analysis. Renew. Energy 87, 376–390.

Gualtieri, G., 2017. Improving investigation of wind turbine optimal site matching through the self-organizing maps. Energy Convers. Manage. 143, 295–311.

Gualtieri, G., 2019a. A comprehensive review on wind resource extrapolation models applied in wind energy. Renew. Sustain. Energy Rev. 102, 215–233. http://dx.doi.org/10.1016/j.rser.2018.12.015, URL https://www.sciencedirect.com/science/article/pii/S1364032118308104.

Gualtieri, G., 2019b. A comprehensive review on wind resource extrapolation models applied in wind energy. Renew. Sustain. Energy Rev. 102, 215–233.

GWEC, Global Wind Energy Council, 2020. Global wind report: Annual market update 2020. URL https://Gwec.Net/Global-Wind-Report-2021/. [Accessed June 24, 2021].

Han, X., Liu, D., Xu, C., Shen, W.Z., 2018. Atmospheric stability and topography effects on wind turbine performance and wake properties in complex terrain. Renew. Energy 126, 640–651.

Högström, U., 1996. Review of some basic characteristics of the atmospheric surface layer. Bound.-Lay. Meteorol. 78 (3), 215–246.

Holtslag, A., 1984. Estimates of diabatic wind speed profiles from near-surface weather observations. Bound.-Lay. Meteorol. 29 (3), 225–250.

Holtslag, M., Bierbooms, W., van Bussel, G., 2017. Extending the diabatic surface layer wind shear profile for offshore wind energy. Renew. Energy 101, 96–110.

Holtslag, M., Bierbooms, W., Van Bussel, G., 2014. Estimating atmospheric stability from observations and correcting wind shear models accordingly. J. Phys. Conf. Ser. 555 (1), 012052, IOP Publishing.

Hong, X., Peng, M., Wang, S., Wang, Q., 2018. Simulating and understanding the gap outflow and oceanic response over the Gulf of Tehuantepec during GOTEX. Dyn. Atmos. Oceans 82, 1–19. http://dx.doi.org/10.1016/j.dynatmoce.2018.01.003.

IEC61400-1, 2005. Wind turbines part 1: Design requirements, 3rd edn. International Electrotechnical Commission, Geneva, Switzerland.

IEC61400-2, 2013. Wind turbines-Part 2. Small wind turbines, 2nd edn. International Electrotechnical Commission, Geneva, Switzerland.

Irwin, J.S., 1979. A theoretical variation of the wind profile power-law exponent as a function of surface roughness and stability. Atmosph. Environ. (1967) 13 (1), 191–194.

Jaramillo, O., Borja, M., 2004. Wind speed analysis in La Ventosa, Mexico: a bimodal probability distribution case. Renew. Energy 29 (10), 1613–1630. http://dx.doi.org/10.1016/j.renene.2004.02.001.

Kalnay, E., 2003. Atmospheric Modeling, Data Assimilation and Predictability. Cambridge University Press.

Kretschmer, M., Schwede, F., Guzmán, R.F., Lott, S., Cheng, P., 2018. Influence of atmospheric stability on the load spectra of wind turbines at alpha ventus. J. Phys. Conf. Ser. 1037 (5), 052009, IOP Publishing.

Lange, M., Focken, U., 2006. Physical Approach to Short-Term Wind Power Prediction, Vol. 208. Springer.

Lee, T.R., Buban, M., 2020. Evaluation of Monin–Obukhov and bulk richardson parameterizations for surface–atmosphere exchange. J. Appl. Meteorol. Climatol. 59 (6), 1091–1107.

Lopez-Villalobos, C., Rodriguez-Hernandez, O., Campos-Amezcua, R., Hernandez-Cruz, G., Jaramillo, O., Mendoza, J., 2018. Wind turbulence intensity at la ventosa, Mexico: A comparative study with the IEC61400 standards. Energies 11 (11), 3007. http://dx.doi.org/10.3390/en11113007.

Lopez-Villalobos, C., Rodriguez-Hernandez, O., Martinez-Alvarado, O., Hernandez-Yepes, J., 2021. Effects of wind power spectrum analysis over resource assessment. Renew. Energy 167, 761–773.

Manwell, J.F., McGowan, J.G., Rogers, A.L., 2010. Wind Energy Explained: Theory, Design and Application. John Wiley & Sons.

Maronga, B., Reuder, J., 2017. On the formulation and universality of Monin–Obukhov similarity functions for mean gradients and standard deviations in the unstable surface layer: Results from surface-layer-resolving large-eddy simulations. J. Atmos. Sci. 74 (4), 989–1010.

Martins, C.A., Moraes, O.L., Acevedo, O.C., Degrazia, G.A., 2009. Turbulence intensity parameters over a very complex terrain. Bound.-Lay. Meteorol. 133 (1), 35–45.
Monin, A., Obukhov, A., 1959. Basic laws of turbulent mixing in the ground layer of the atmosphere (osnovne zakonomernosti turbulentnogo peremeshivaniya v prizemnom sloe atmosfery). Tech. rep., AMERICAN METEOROLOGICAL SOCIETY BOSTON MA.
Moraes, O.L., Acevedo, O.C., Degrazia, G.A., Anfossi, D., da Silva, R., Anabor, V., 2005. Surface layer turbulence parameters over a complex terrain. Atmos. Environ. 39 (17), 3103–3112.
Motta, M., Barthelmie, R.J., Vølund, P., 2005. The influence of non-logarithmic wind speed profiles on potential power output at danish offshore sites. Wind Energy Int. J. Progress Appl. Wind Power Convers. Technol. 8 (2), 219–236.
Nadeau, D.F., Pardyjak, E.R., Higgins, C.W., Parlange, M.B., 2013. Similarity scaling over a steep alpine slope. Bound.-Lay. Meteorol. 147 (3), 401–419.
Newman, J.F., Klein, P.M., 2014. The impacts of atmospheric stability on the accuracy of wind speed extrapolation methods. Resources 3 (1), 81–105.
Nickerson, E.C., Smiley, V.E., 1975. Surface layer and energy budget parameterizations for mesoscale models. J. Appl. Meteorol. 14 (3), 297–300.
Obukhov, A., 1971. Turbulence in an atmosphere with a non-uniform temperature. Bound.-Lay. Meteorol. 2 (1), 7–29.
Optis, M., Monahan, A., Bosveld, F.C., 2016. Limitations and breakdown of Monin–Obukhov similarity theory for wind profile extrapolation under stable stratification. Wind Energy 19 (6), 1053–1072.
Ouammi, A., Sacile, R., Mimet, A., 2010. Wind energy potential in liguria region. Renew. Sustain. Energy Rev. 14 (1), 289–300.
Petersen, E.L., Mortensen, N.G., Landberg, L., Højstrup, J., Frank, H.P., 1998. Wind power meteorology. Part I: Climate and turbulence. Wind Energy Int. J. Progress Appl. Wind Power Convers. Technol. 1 (S1), 25–45.
Radünz, W.C., Sakagami, Y., Haas, R., Petry, A.P., Passos, J.C., Miqueletti, M., Dias, E., 2020. The variability of wind resources in complex terrain and its relationship with atmospheric stability. Energy Convers. Manage. 222, 113249.
Raupach, M.R., Finnigan, J.J., Brunet, Y., 1996. Coherent eddies and turbulence in vegetation canopies: the mixing-layer analogy. In: Boundary-Layer Meteorology 25th Anniversary Volume, 1970–1995. Springer, pp. 351–382.
Rehman, S., Al-Hadhrami, L.M., Alam, M.M., Meyer, J.P., 2013. Empirical correlation between hub height and local wind shear exponent for different sizes of wind turbines. Sustain. Energy Technol. Assess. 4, 45–51.
Rehman, S., Alam, M.M., Alhems, L.M., 2018. A review of wind-turbine structural stability, failure and alleviation. Adv. Civil, Environ. Mater. Res. (ACEM18) 27–31.
Romero-Centeno, R., Zavala-Hidalgo, J., Gallegos, A., O'Brien, J.J., 2003. Isthmus of Tehuantepec wind climatology and ENSO signal. J. Clim. 16 (15), 2628–2639.
Roque, L.A., Paiva, L.T., Fernandes, M.C., Fontes, D.B., Fontes, F.A., 2020. Layout optimization of an airborne wind energy farm for maximum power generation. Energy Rep. 6, 165–171.
Rotach, M.W., Calanca, P., Graziani, G., Gurtz, J., Steyn, D.G., Vogt, R., Andretta, M., Christen, A., Cieslik, S., Connolly, R., et al., 2004. Turbulence structure and exchange processes in an alpine valley: The riviera project. Bull. Am. Meteorol. Soc. 85 (9), 1367–1386.
Rotach, M.W., Zardi, D., 2007. On the boundary-layer structure over highly complex terrain: Key findings from MAP. Q. J. R. Meteorol. Soc. J. Atmospheric Sci. Appl. Meteorol. Phys. Oceanogr. 133 (625), 937–948.
Sathe, A., Bierbooms, W., 2007. Influence of different wind profiles due to varying atmospheric stability on the fatigue life of wind turbines. J. Phys. Conf. Ser. 75 (1), 012056, IOP Publishing.
Sathe, A., Mann, J., Barlas, T., Bierbooms, W., Van Bussel, G., 2013. Influence of atmospheric stability on wind turbine loads. Wind Energy 16 (7), 1013–1032.
Schulz, C., Klein, L., Weihing, P., Lutz, T., Krämer, E., 2014. CFD studies on wind turbines in complex terrain under atmospheric inflow conditions. J. Phys. Conf. Ser. 524 (1), 012134, IOP Publishing.
Schwartz, M., Elliott, D., 2006. Wind shear characteristics at central plains tall towers. Tech. rep., National Renewable Energy Lab.(NREL), Golden, CO (United States).
Serafin, S., Adler, B., Cuxart, J., De Wekker, S.F., Gohm, A., Grisogono, B., Kalthoff, N., Kirshbaum, D.J., Rotach, M.W., Schmidli, J., et al., 2018. Exchange processes in the atmospheric boundary layer over mountainous terrain. Atmosphere 9 (3), 102.
Serban, A., Paraschiv, L.S., Paraschiv, S., 2020. Assessment of wind energy potential based on Weibull and Rayleigh distribution models. Energy Rep. 6, 250–267.
Smith, K., Randall, G., Malcolm, D., Kelley, N., Smith, B., 2002. Evaluation of wind shear patterns at midwest wind energy facilities. Tech. rep., National Renewable Energy Lab., Golden, CO (US).
Stull, R.B., 1988. An Introduction to Boundary Layer Meteorology, Vol. 13. Springer Science & Business Media.
Tampieri, F., 2017. Turbulence and Dispersion in the Planetary Boundary Layer. Springer.
Tennekes, H., 1973. Similarity laws and scale relations in planetary boundary layers. In: Workshop on Micrometeorology, Vol. 177. Amer. Meteor. Soc, p. 216.
Thakur, A., Panigrahi, S., Behera, R., et al., 2016. A review on wind energy conversion system and enabling technology. In: 2016 International Conference on Electrical Power and Energy Systems (ICEPES). IEEE, pp. 527–532.
Đurišić, v., Mikulović, J., 2012. A model for vertical wind speed data extrapolation for improving wind resource assessment using WAsP. Renew. Energy 41, 407–411.
Van Sark, W.G., Van der Velde, H.C., Coelingh, J.P., Bierbooms, W.A., 2019. Do we really need rotor equivalent wind speed? Wind Energy 22 (6), 745–763.
Vasel-Be-Hagh, A., Archer, C.L., 2017. Wind farm hub height optimization. Appl. Energy 195, 905–921.
Vestas, 2015. 2MW platform. http://nozebra.ipapercms.dk/Vestas/Communication/Productbrochure/2MWbrochure/2MWProductBrochure/, Accessed: 2022-02-06.
Wagner, R., Cañadillas, B., Clifton, A., Feeney, S., Nygaard, N., Poodt, M., St Martin, C., Tüxen, E., Wagenaar, J., 2014. Rotor equivalent wind speed for power curve measurement–comparative exercise for IEA wind annex 32. J. Phys. Conf. Ser. 524 (1), 012108, IOP Publishing.
Wagner, R., Courtney, M., Gottschall, J., Lindelöw-Marsden, P., 2011. Accounting for the speed shear in wind turbine power performance measurement. Wind Energy 14 (8), 993–1004.
Wharton, S., Lundquist, J.K., 2012. Atmospheric stability affects wind turbine power collection. Environ. Res. Lett. 7 (1), 014005.
Wharton, S., Newman, J., Qualley, G., Miller, W., 2015. Measuring turbine inflow with vertically-profiling lidar in complex terrain. J. Wind Eng. Ind. Aerodyn. 142, 217–231.
Willmott, C.J., 1981. On the validation of models. Phys. Geogr. 2 (2), 184–194.
Zannetti, P., 2013. Air Pollution Modeling: Theories, Computational Methods and Available Software. Springer Science & Business Media.
Zhan, L., Letizia, S., Valerio Iungo, G., 2020. LiDAR measurements for an onshore wind farm: Wake variability for different incoming wind speeds and atmospheric stability regimes. Wind Energy 23 (3), 501–527.
Zilitinkevich, S., Calanca, P., 2000. An extended similarity theory for the stably stratified atmospheric surface layer. Q. J. R. Meteorol. Soc. 126 (566), 1913–1923.
Zoumakis, N., Kelessis, A., 1991. Methodology for bulk approximation of the wind profile power-law exponent under stable stratification. Bound.-Lay. Meteorol. 55 (1), 199–203.